Growth-deviation model to understand the perceived variety of falling snow

J. Nelson

Atmos. Chem. Phys. Discuss., 8, 4407–4437, 2008
www.atmos-chem-phys-discuss.net/8/4407/2008/

Atmospheric Chemistry and Physics Discussions

Growth-deviation model to understand the perceived variety of falling snow

J. Nelson

College of Science and Engineering, Ritsumeikan University, Nojihigashi 1-1-1, Kusatsu 525-8577, Japan

Received: 20 December 2007 – Accepted: 9 January 2008 – Published: 4 March 2008

Correspondence to: J. Nelson (jnelson@se.ritsumei.ac.jp)

Published by Copernicus Publications on behalf of the European Geosciences Union.

Abstract

What is the source of snow-crystal variety? This question is answered using a model of snow-crystal growth in a cloud. In the model, crystals start under various initial cloud-crystal conditions, and then encounter growth perturbations from random air-temperature deviations along simple crystal trajectories. To obtain distributions of these deviations, I analyzed recent high-resolution measurements of cloud updrafts and temperatures. The trajectories and distributions are used to estimate the number of possible snow crystal shapes, to a given viewing resolution, from a range of initial conditions. The logarithm of this number, defined here as the perceived shape variety or "diversity", is dominated not by the range of conditions, but rather by the air-temperature deviations along a trajectory. This qualitative result is independent of the viewing resolution. Thus, temperature deviations are the main source of crystal diversity. When plotted against the crystal's initial temperature (here –11 to –19°C), the curve is mitten-shaped, with a main peak at –15.4°C and a smaller, sharper peak near –14.4°C. The mitten shape arises from temperature trends in the crystal's terminal fallspeed and prism-face growth rate. Specifically, the two diversity peaks are due to maxima in growth-rate sensitivity to temperature near –15.4 and –14.0°C. Applying the results to all snow crystals ever formed, then, to 1-μm resolution, all crystals that began near –15°C would appear unique, but some that began near –11°C would not.

1 Introduction

Snow crystals are admired for their symmetry and variety. The source of the apparent six-fold symmetry is understood to arise from the ice crystal structure and growth mode (Frank, 1982; Nelson, 2005), but the source of the perceived variety has not been examined quantitatively. Here we use results from recent snow and cloud studies to better understand this variety.

The number of possible snow crystal shapes is estimated to be immense (Knight

ACPD

8, 4407–4437, 2008

and Knight, 1973; Hallett, 1984). However, these estimates are highly inconsistent[1] and they do not address important details such as the cloud conditions and growth process. Bentley (1901), addressing the cause of the variety, wrote that the various crystal features come from the various "atmospheric layers" passed through during the crystal descent. Later, Nakaya (1954), showed that the basic habit (e.g., columnar or tabular) arose from the crystal's growth temperature, and that the intricate features arose as humidity increased. But for a crystal falling through a cloud, the main cause of the perceived variety remains unknown.

This cause is determined as follows. We define in Sect. 2 a growth-process-based measure of perceived shape variety, hereafter diversity, then, in Sect. 3, determine the crystal-cloud influences on growth, and finally apply the measure to these influences. In Sect. 4, we analyze variations to the initial crystal and trajectory parameters, then, in Sect. 5, analyze deviations in updraft speed and air temperature along each trajectory. These variations and deviations are not used to predict specific crystal shapes; rather, they are used to estimate when observable changes occur to a given, yet unspecified, shape. The results in Sect. 6 indicate that most of the diversity comes from the deviations, yet the magnitudes are much less than those from previous estimates.

2 Diversity and growth

Here we define a shape diversity S and then apply it to snow crystal growth. The key growth variable is the temperature-dependence of the prism-face growth rate.

2.1 Definition of diversity

Let S equal the logarithm of the number of possible distinguishable shapes (defined below) that can arise during growth. Hence, if each shape is nearly equally likely, then

[1] The first estimate can be shown to exceed about $10^{3000000}$, but the second is about 10^{30000}, a difference of ~three million orders of magnitude.

cloud conditions with a large S can produce many shapes. The logarithm is useful because the number of possible shapes can vary by many orders of magnitude. Moreover, variety is conceptually similar to entropy, which is proportional to the logarithm of the number of possible *states* instead of distinguishable *shapes*. But to proceed, we need a way to distinguish crystals.

2.2 Distinguishing features

Ideally, two crystals are perceived as distinguishable if one cannot superimpose one crystal's image over the other (viewed as in Fig. 1) without noticing a change in either image. That is, two crystals are "the same" to some resolution if the positions of the perimeter and interior lines match when viewed at that resolution. These lines mark regions, hereafter "features" (e.g., Fig. 1a–c, right side), where growth produced a sharp bend in the surface, causing a contrast in light reflection. But instead of examining images, we use the final crystal size to estimate the number of times during growth that a resolvable feature could have started. In this way, the diversity will depend, as it should, on the assumed resolution.

2.3 Focus on prism-face growth

The initial position of growth-induced features likely result from growth changes on the outermost faces. In general, these faces can be either basal or prism faces, depending on the temperature. But here we focus on the commonly viewed tabular snow crystals that form between ~–9 and –22°C. The prism faces grow fastest in this range, so we assume that prism growth rates determine when new features arise. This temperature restriction is useful because it simplifies the analysis, but it means that the results are valid only when the crystals remain between about –9 and –22°C.

When the growth-rate slows, not only does the diameter increase at a slower rate, but the prism-face area changes, possibly introducing new features. For a slightly hollowed prism face (e.g., Fig. 2a–c), the pits decrease in size, producing "interior" ridges and

wiggles. For a branched crystal (e.g., Fig. 2d–f), the branches widen at the tip, thus altering the perimeter. Other features can similarly arise from growth changes (Nelson, 2005).

2.4 Growth changes from temperature changes

The growth rate of the prism face r is proportional to the deviation of the vapor pressure above that of equilibrium, which is proportional to relative humidity. As temperature-dependent surface processes also affect r, both humidity and temperature can independently affect growth. But for the local, in-cloud conditions around a crystal, the humidity is often near the temperature-dependent value for liquid water in equilibrium. This is because snowfall-producing clouds often contain significant liquid water. In such mixed-phase clouds, measurements (Korolev and Isaac, 2006; Siebert et al., 2003)[2] and theory (Shaw, 2000) suggest that the humidity stays near liquid-water saturation. Hence, as a first approximation, we will assume that each crystal grows in an environment in which the humidity is at liquid-water saturation. As such, the air temperature controls r. This rate has a peak near –14.8°C (Fig. 3), which suggests that we must carefully track the temperature to estimate when growth features can arise.

3 Crystal trajectories and diversity influences

If collisions and crystal-scale gradients in humidity and temperature are ignored, the above arguments mean that the initial crystal properties and temperature history determine the final crystal form. We now study these influences in detail.

[2] In the former, measurements were averaged over 100 m. In the latter, air temperature and liquid water content at 15-cm resolution were correlated as if the droplets grew or evaporated to stay near equilibrium.

3.1 Initial crystals and reference trajectories

Most snow crystals are thought to start as frozen, nearly spherical droplets. Although frozen droplets have various characteristics that may affect subsequent growth, this is poorly understood. So, we characterize the initial crystal solely by its diameter d_0. In contrast, we can consider details of the ensuing temperature history. Temperature changes along a crystal trajectory are due to air-temperature inhomogeneities DT_{ai} and the altitude-dependent air temperature. The latter contribution to temperature history is the sum of that from 1) slowly varying altitudes for a crystal in an updraft of constant (path-average) speed, and 2) DT_{Du} from altitude deviations due to updraft-speed deviations Du. Horizontal motion is ignored.

To account for these temperature deviations, we write the crystal temperature at time t as $T(t)=T(\mathrm{z}(t))+DT(t)$, where $T(\mathrm{z}(t))$ is the temperature for a crystal lofted in an updraft with the path-averaged speed $\bar{u}$, in which the altitude is $z(t)$, and $DT(t)$ is the total temperature deviation along a trajectory ($=DT_{ai}+DT_{Du}$). A given trajectory $\mathrm{z}(t)$, hereafter a "reference" trajectory, changes as $dz/dt=\bar{u}-v$, where v is the crystal's terminal fallspeed and $T(z)$ decreases with z as $dT(z)/dz \equiv T' = -7\times10^{-3}\,^{\circ}$C/m, a typical environmental lapse rate. An actual updraft has speed $\bar{u}+Du(t)$, but Du is used only to estimate DT_{Du}, not for calculating trajectories. These and other model parameters are sketched in Fig. 4.

The duration of a trajectory depends on $\bar{u}$ and how quickly the fallspeed v increases. The latter depends on crystal shape, with v increasing slowest for the crystals that, surprisingly, grow the fastest (Fig. 3). These crystals fall slowest because, as tabular crystals fall broadside to the airflow, the broadest (and thinnest) crystals expose the greatest area to the airflow, thus having the greatest drag force. Hence, the crystals that grow the fastest also fall the slowest, and end up with the longest growth times.

ACPD
8, 4407–4437, 2008

3.2 Three influences on diversity

A reference trajectory begins when a crystal nucleates at temperature T_0 from a droplet of diameter d_0. Here $-11 \geq T_0 \geq -19$ °C. Typically, $\bar{u}$ exceeds the fallspeed of the micron-sized frozen droplets, so the crystal initially rises and thus cools. When v reaches $\bar{u}$, the crystal has its maximum altitude[3] and minimum T, and thereafter falls towards cloudbase at the warmer temperature T_f. (We assume growth stops when the crystal reaches cloudbase, though some growth occurs below cloudbase where the humidity is between ice and liquid saturation.) The temperature deviations superimpose on the reference trajectories. Thus, we consider three influences on crystal variety: the initial diameter, the reference trajectory, and temperature deviations.

Variations in these influences are treated independently. Although not exact, this makes it easier to discuss each influence separately. In this case, the number of possible forms $N \approx N_0 N_{\text{ref}} N_{\text{dev}}$, where N_0 is the number of possible forms due solely to variations of the initial crystal diameter, and N_{ref} and N_{dev} are the numbers for the reference trajectories and deviations. The shape diversity $S \equiv \text{Log}_{10}[N]$, and so

$$S \approx S_0 + S_{\text{ref}} + S_{\text{dev}}, \tag{1}$$

where $S_0 = \text{Log}_{10}[N_0]$ and likewise for the other two numbers.

4 Influence of initial crystal and reference trajectories

To evaluate S_0, S_{ref}, and S_{dev}, we track the crystal diameter d, temperature T, and pathlength L (air depth the crystal falls through) along reference trajectories. Here we use the reference trajectories to analyze S_0 and S_{ref}. A trajectory is determined by d_0,T_0, T_f, $\bar{u}$, and v. But v depends on d and the crystal's shape, which are determined by d_0 and $T(t)$. Thus, reference trajectories depend only on d_0, T_0, $\bar{u}$, and T_f (and

[3] For updrafts considered here, the altitude increase is typically less than 100 m.

dependence on d_0 is weak). Upon exiting cloudbase, the crystal has diameter d_f and total pathlength L_f. Calculation details are in Appendix A.

4.1 Distinguishable classes for initial diameters and reference trajectories

For a given set of values d_0, T_0, $\bar{u}$, and T_f, a variable, say $\bar{u}$, can be varied by up to $\delta\bar{u}$ and the final crystal forms will be indistinguishable (neglecting temperature deviations). When $|d\bar{u}|>\delta\bar{u}$, the resulting crystal will have a feature displaced by at least *res* from that on the original ($|d\bar{u}|=0$) crystal. To determine δd_0, δT_0, $\delta\bar{u}$, and δT_f, we consider changes to d_f, a common feature that is relatively sensitive to the temperature history. If variable X with value x results in d_f, then value $x+\delta X$ results in $d_f \pm 2res$. So, if d_f is sensitive to X, then δX will be relatively small. Crystals within $d_0\pm\delta d_0$, $T_0\pm\delta T_0$,$\bar{u}\pm\delta\bar{u}$, and $T_f\pm\delta T_f$ are said to be in the same "d_0-*reference*" class because they all would be perceived as indistinguishable.

4.2 Number of distinguishable d_0-*reference* classes

To estimate S_0 and $S_{\rm ref}$, we also need a typical range of each variable. Call these Δd_0, ΔT_0,$\Delta\bar{u}$, and ΔT_f. If the variables are independent, then the number of possible distinguishable crystals due to changes in d_0 is $N_0=\Delta d_0/\delta d_0$, which also equals the number of distinguishable d_0 classes. That for the reference classes is $N_{\rm ref}=(\Delta T_0/\delta T_0)\times(\Delta\bar{u}/\delta\bar{u})\times(\Delta T_f/\delta T_f)$. Using $\{\Delta d_0,\ \Delta T_0,\ \Delta\bar{u},\ \Delta T_f\}=\{39\ \mu$m, 10°C, 0.24 m/s, 8°C$\}$ and calculating the trajectories, the shape diversities S_0 and $S_{\rm ref}$ average to 1.2 and 8.7 (see Table 1). S_0 is small because d_0 has a significant influence only at the start; for example, a crystal that begins 2–μm larger will end about 2-μm larger. This suggests that $S_0\approx{\rm Log}_{10}[\Delta d_0/2res]=1.3$. The value is instead 1.2 because d also affects v. $S_{\rm ref}$ is much larger, mainly because d_f is sensitive to T_0 and $\bar{u}$, both of which affect T (and hence r) throughout the trajectory. In contrast, T_f only affects L_f, thus adding relatively little to $S_{\rm ref}$.

ACPD
8, 4407–4437, 2008

5 Influence of temperature deviations

Let each d_0-*reference* class represent a certain (yet unspecified) shape, and consider temperature deviations that may produce shape changes. As a crystal falls, the continuously varying DT will continuously alter the crystal's growth features. But there will be some average duration between *relevant* DT changes, that is, between DT changes that can produce distinguishable changes to the crystal features.

Once a feature forms, it can grow and change. For example, if a sidebranch sprouts and no further DT deviations occur, subsequent growth is determined by the rest of the trajectory. Otherwise, subsequent relevant DT deviations will affect the shape according to when they occur. Thus, we must estimate the number of relevant deviations and when each one may occur. We first address the former.

5.1 Number of relevant deviations

We set a temperature-based criterion for the relevant deviations, then estimate how often the criterion is satisfied for a given crystal path. In time dt, a crystal falls through pathlength $dL=vdt$ as its outermost prism faces advance by $dR=rdt$, where r is the prism-face growth rate (Fig. 3). ($dL \neq dz$ unless $\bar{u}=0$.) A temperature differing by DT_i produces a growth-rate change $dr_i=r'DT_i$, where "i"="ai" or "Du" and $r' \equiv dr/dT$. The size of the surface perturbation thus produced is $d^2R_i=dr_i dt$. (For a lateral deviation (e.g., Fig. 2a), the growth rate is unknown, so we use r as an approximation.) Integrating d^2R_i between depth L_t at time t and L_t+L gives δR_i:

$$\delta R_i(L_t, L) = \int_{L_t}^{L_t+L} r'(x) DT_i(x) v^{-1}(x) \mathrm{d}x \equiv r' v^{-1} \Sigma_i(L_t, L), \quad (2)$$

where the T changes are small enough to remove r' and v from the integrand. The number of relevant deviations in Σ_i is nearly independent of L_t, so we can ignore this dependence. For a surface perturbation to enlarge, eventually to exceed *res*, it must receive more vapor flux than adjacent regions. This suggests that δR must exceed λ

ACPD
8, 4407–4437, 2008

the vapor mean-free path, which we fix at 0.08 μm (λ varies only slightly with T and z). Thus, from Eq. (2), a surface perturbation can become a feature (i.e., relevant) when

$$\Sigma_i(L) \geq \frac{\lambda v}{r'} \equiv p. \quad (3)$$

The parameter p greatly influences S_{dev} due to the sensitivity of v and r' to T. During growth, p generally increases due to the increase of v. For crystals with T_0=–15°C, much of the growth occurs with p~0.018°C m. In contrast, crystals with T_0 near –11 and –19°C have typical p values about 10 and 20 times larger.

5.2 Distribution functions from stratus clouds

The frequency that Eq. (3) is satisfied depends on p and L. To handle this dependence, we define peak distribution functions $F_i(p)$ as the number of peaks exceeding p in unit L.

To estimate $F_i(p)$, I used data from horizontal flight paths in stratus clouds with T<0°C (the only available data). The DT_{ai} values were direct measurements, but DT_{Du} required integration of Du to get the altitude deviation Dz, from which DT_{Du}=$T'Dz$. (The integration introduced factor v^{-1} into δR_{Du}, and thus F_{Du} also depends on v.) Then I integrated DT_i to obtain Σ_i, from which the F_i were derived. Details are in Appendix C.

The F_{ai} functions from two cloud datasets decayed as $p^{-0.66}$ and agreed within a factor of two, even though the clouds had different temperature averages and the measurements were done differently (Fig. 5). In contrast, only one cloud dataset was available for F_{Du}, and the values decayed as $p^{-0.50}$. The reason F_i decay with exponents 2/3 and 1/2 is unclear, but, as expected, F_i decrease with increasing p values. This decrease, together with the crystal size, strongly affects the diversity.

5.3 Total pathlength and crystal size

For constant p and v, the number of times n that a temperature deviation can produce a new feature is the product of the total pathlength with the distribution functions. But

only some fraction χ of the deviations will grow into a new feature, so

$$n = \chi L_f(F_{ai}(p) + F_{Du}(p, v)). \quad (4)$$

Each of these n features could have been born when the crystal radius was at any one of m distinct radial positions on the crystal, where

$$m \equiv \frac{d_f}{2 \cdot res}. \quad (5)$$

That is, there are m resolvable growth intervals. m and n are used below to calculate S_{dev}. Although m depends on both the trajectory (through d_f) and the resolution, n depends only on the trajectory.

5.4 Estimates of L_f, d_f, n, and m

The reference trajectories were used to estimate L_f and d_f (Table 1), from which n and m were calculated (Table 2). The L_f values increased as T_0 decreased, most rapidly as T_0=–15°C was approached from lower heights. This is because v decreases as $T_0 \rightarrow$–15°C (Fig. 3). Moreover, L_f could greatly exceed the cloud thickness when $\bar{u}$ was at least 0.25 m/s and T_0 was near –15°C. In addition, near this temperature d_f was largest. The reason for the peak in d_f is not only the peak in r, but also the minimum in v. Similarly, the peak in n near –15°C has two causes: the trend in L_f and the peaks in r' at –14.0 and –15.4°C (Fig. 3). In Sect. 6.2 below, we integrate $dn = \chi(F_{ai} + F_{Du})dL$ for more precise analysis and show that a double-peak exists.

5.5 Combinatorial method for S_{dev}

From the calculated trajectory, a crystal has n features that can arise in m resolvable growth intervals, and each feature may be born during either a growth spurt or lull,

ACPD
8, 4407–4437, 2008

meaning that one of two possible features can grow from each interval[4]. The resulting number of feature combinations is a standard combinatorial calculation (Feller, 1968):

$$N_{\text{dev}} = \binom{m}{n} 2^n = \frac{m!}{n!(m-n)!} 2^n. \quad (6)$$

As $m \gg 1$, $n \gg 1$, and $m-n \gg 1$ (Table 2), Stirling's factorial approximation can be used:

$$N_{\text{dev}} \approx \frac{2^n}{\sqrt{2\pi n(1-\frac{n}{m})}} \frac{(\frac{m}{n}-1)^n}{(1-\frac{n}{m})^m}. \quad (7)$$

When $m \gg n$, N_{dev} approaches $(2\pi n)^{-1/2}(2me/n)^n$, showing that N_{dev} increases rapidly when either m or n increases. In this case

$$S_{\text{dev}} \approx n \cdot \text{Log}_{10}[\frac{2m \cdot e}{n}] - \frac{1}{2}\text{Log}_{10}[2\pi n]. \quad (8)$$

When $res < 4\,\mu$m, Eq. (8) is accurate to within 1–3% of the value derived from Eq. (6).

6 Discussion

6.1 The main source of snow crystal variety

As $\text{Log}_{10}[2me/n] > 1$ and $n \gg 1/2$ (Table 2), Eq. (8) suggests that S_{dev} exceeds n, which exceeds $S_0 + S_{\text{ref}}$ for all T_0. Furthermore, according to the dependence of S_0, S_{ref}, and S_{dev} on *res*, this finding is independent of viewing resolution, provided *res* is not so large that $m < n$. Hence, of the three factors, temperature deviations caused most of the variety. This suggests that our impression of seemingly endless snow-crystal

[4] This assumes $m \geq n$, which holds for *res* less than about 5 μm, depending on the cloud conditions. For larger *res*, one would have to set n to equal m, and there may be more than two possible features from each resolvable growth interval.

variety arises from the large number of relevant deviations, which is due to the highly fluctuating nature of T and u in clouds (See, e.g., Fig. 7).

6.2 Further analyses: the S_{dev} "mitten" curve

A plot of S_{dev} versus T_0 reveals a curve in a mitten-like shape (Fig. 6). In particular, in the baseline case, the curve has a larger, broader peak near –15.4°C and a smaller, narrower peak near –14.4°C. This mitten shape comes from n, which is double-peaked because r' peaks on both sides of the growth-rate peak near –14.8°C. The lower-temperature peak is larger partly because only lower-temperature crystals experience both r' peaks. In addition, crystals that start at lower temperatures have greater S_{dev} due to their larger d_f, which is partly due to their longer L_f. But these effects are greatly reduced when the cloudbase is only 1°C warmer than T_0, making the curve more nearly symmetric about the peak in growth rate near –14.8°C.

The results in Fig. 6 also can explain why the biggest crystals seem the most elaborate. Clearly, S_{dev} increases with size due to the influence of m (Eq. (8)). But there is another reason. The peak in size is due to the maximum in r (and minimum in v), whereas the S_{dev} peak is largely due to the nearby peaks in r'. This is suggested by the correlation between the double peaks in S_{dev} and r'. So, because the r peak is near the r' peaks, larger crystals (larger d_f) have greater S_{dev} and thus are more elaborate. To better understand the T_0 dependence, consider how r, r', and v affect S_{dev}. In the baseline case, S_{dev} changes from 41.3 at –11.0°C to 479.9 near –15.4°C. But when the T_0=–11°C case was run with $r(T)$ evaluated 4.4°C lower (to equal that of a –15.4°C crystal), the resulting S_{dev} was 64.0, an increase of 18.7. If instead v was evaluated 4.4°C lower, the value of S_{dev} increased by 33.4. However, when r' was evaluated 4.4°C lower, S_{dev} increased by 60.2, showing that r' had the largest effect. (When r, r', and v were all 4.4°C lower, S_{dev} went up even more – by 366.1.) Hence, big crystals can appear more complex both for the obvious reason, that they have more places for features to originate, and because the growth-rate sensitivity to temperature is high near temperatures at which big crystals grow.

ACPD
8, 4407–4437, 2008

6.3 Sensisitivity and uncertainty

The analysis shows that S_{dev} is relatively insensitive to T_f but sensitive to $\bar{u}$. A decrease in T_f decreased S_{dev} for all crystals, particularly those that started near cloudbase. But the decrease is relatively small, and peak temperatures shifted only slightly to lower temperatures (Fig. 6, stars). The latter occurred because a raising of cloudbase decreases L_f. A greater decrease in S_{dev} occurred when $\bar{u}$ decreased to 0.03 m/s. In this case, the peak temperatures shifted to lower values. The lower values are due to the shorter L_f values, and the decrease in peak temperatures occurs because T_0 must decrease to have the same minimum temperature, where much of the growth occurs.

In contrast, S_{dev} is sensitive to *res* and χ. If the resolution is coarser, then *res* is larger, resulting in less diversity. For example, Fig. 6 shows that the peak diversity decreases by about 170 when *res* increases from 1 to 4 μm. This is due to a decrease in m. Even greater sensitivity comes from χ due to the proportionality of n to χ. For example, when χ decreased from 1/2 to 1/8, the peak diversity decreased from 486 to 160. The value χ=0.5 used in the baseline case is uncertain and may depend on crystal form, feature type, and the size and rate of the deviation. Analysis suggests that χ is larger at faster growth rates, particularly when the feature is a sidebranch (Nelson, 2005), and χ may be nearly zero for small, slow-growing crystals that have not yet hollowed (e.g., Fig. 1a). So, χ=0.5 may overestimate S_{dev}, at least at slow growth rates.

6.4 Neglected influences on diversity

By how much might the results change if we had considered the influence from humidity? If data were available on small-scale deviations of humidity from liquid-water saturation and the resulting growth-rate response, one could use the same method as that used here for T. However, unlike T, humidity has no altitude-related contribution, which is large in the temperature case: $F_{ai} > F_{Du}$ for a range of v values (see Fig. 5). This difference, together with the finding that these humidity deviations are typically

small, suggests that the humidity contribution should be less than that for temperature.

Other potentially major sources of variety are the initial crystal's structure and close passages/collisions of droplets. When the growth rate is low (e.g., ∼–11 and –19°C), step-producing defects can greatly affect the growth rate of a prism face (Wood et al., 2001). Moreover, crystals nucleated under different conditions can end up with different shapes (Yamashita, 1973). But we have little knowledge of either influence. Finally, droplets may pass close to, and land on, a crystal, thus locally changing the humidity and even the temperature (when the droplet freezes). Such effects seem significant in some cases (Hallett and Knight, 1994), though quantitative treatment is not presently possible.

6.5 Errors from model idealization

The use of temperature and updraft data from horizontal paths may misrepresent the deviations experienced by rising and falling crystals. But high-resolution data along the vertical does not yet exist. Also, snow clouds can have regions with $\bar{u}$ values much larger than the values here (Wolde and Vali, 2001); however, larger $\bar{u}$ values would produce unrealistically large crystals, so the baseline-case $\bar{u}$ here may be a reasonable average. Finally, data on $r$and v cover only idealized, constant conditions. In an actual cloud, side-to-side (leaf-like) falling motion and changing temperatures may alter r and v. So, although much remains unknown about clouds and snow, the treatment here is a realistic first step.

6.6 Comparison to previous estimates

For the above case in which res=1 μm, the maximum value of S is about 500, which, though large, is much less than previous estimates. Knight and Knight (1973) estimated the number of molecules in a typical snow crystal and then considered, but did not evaluate, the number of ways these molecules could be arranged. A lower bound of this number is derived from Eq. (6) by substituting for m a crystal radius divided by

the water-molecule diameter and summing over all n values (0 to m). The result is 3^m, which, for a radius of 3 mm, gives an S value of 3×10^6. In contrast, Hallett (1984) assumed a resolution 3×10^4 times larger (10 μm), yet calculated the larger number of $S=5\times10^6$. His treatment involved consideration of 10^4 "points" on the crystal, apparently each of which could have grown in one of 20 humidity classes and one of 50 temperature classes. Based on these assumptions, the number of possible crystals should instead be $(20\times50)^{10000}$, which gives $S=3\times10^4$ – clearly inconsistent with the earlier estimate. Both of these earlier treatments gave S values vastly larger than those found here, mainly because they ignored limitations from the growth process. This huge difference in numbers has implications for the following question.

6.7 Comparison to observations: Should every snow crystal look unique?

An observational test of the mitten curve is impractical unless *res* is very large. So instead, we check to see if the numbers are reasonable by estimating the likelihood that all crystals in some collection appear unique.

Consider a large, heavy snowstorm that deposits a liquid-water-equivalent snow depth of 3 cm (~20-inches of snow) over a land area of 10^4 km^2. In total, this equals $\sim3\times10^{11}$ kg of water. Assuming each crystal is 10^{-9} kg, this amount of snow contains $\sim3\times10^{20}$ crystals, of which $N_{cry}\sim3\times10^{18}$ may be reasonably symmetric at cloudbase[5]. N_{cry} could be compared to N; however, N varies with the cloud and crystal parameters (Fig. 6). So we instead consider each d_0-*reference* class separately.

If all crystals are equally likely to be in each class, then the number of crystals per class is $N_{cl}\sim N_{cry}/10^{S_0+S_{ref}}$. Using S_0 and S_{dev} from Table 1, $N_{cl}=4\times10^8$. The probability $pd(i)$ that all crystals in class i are unique can be estimated by counting the number

[5] Large crystals with perfect symmetry (at typical viewing resolution) are unlikely. But we can average the features over all 30°-angle sectors, which are ideally equivalent. Conversely, we could consider each such sector independently, and find the probability that any two sectors on different crystals are the same. This case would involve about $12\times3\times10^{20}$ sectors.

of ways that this class can have only unique crystals. This problem is equivalent to the well-known "birthday paradox", which is the (surprisingly low) probability that all people in a group have birthdays on different days of the year. Here $N_{cl} \gg 1$ and $N_{dev}(i) \gg 1$, so we can use Feller's (1968) approximation:

$$pd(i) \approx e^{-\frac{N_{cl}^2}{2N_{dev}(i)}}. \quad (9)$$

For all crystals to be unique, each class can have only unique crystals. Thus, pd_{all}, the probability that all crystals are unique, should be the product of all $pd(i)$. This means that $pd_{all} < pd(0)$, where $i=0$ is the class with the smallest pd. From Eq. (9), this class has the smallest N_{dev}; hence, it should have a warm T_0, a low $\bar{u}$, and a cold T_f. For example, if $T_0 = -11^{\circ}$C, $\bar{u} = 0.02$ m/s, and $T_f = -10.5^{\circ}$C, calculation shows $N_{dev} \approx 5 \times 10^{16}$. Putting this N_{dev} and N_{cl} into Eq. (9) gives $pd(0) = 0.2$, suggesting that large snowstorms have enough crystals for some of the smaller crystals to appear as copies. Considering the uncertainties, this number is imprecise; however, the claim that $pd_{all} \gg 1$ strengthens if we either use a larger *res* or if we included *all* snow crystals that have *ever* fallen on Earth. In the latter case, N_{cl} increases by many orders of magnitude because $10^{S_0+S_{ref}}$ hardly changes yet N_{cry} increases from $\sim 10^{18}$ to $\sim 10^{33}$ (Knight and Knight, 1973). This greatly decreases $pd(0)$. In contrast, if a class has crystals with $T_0 \sim -15.4^{\circ}$C, then $pd \approx 1$ even if we consider all such crystals that have ever fallen. (Here the exponent is $\sim -10^{-433}$, making $pd = 1 - 10^{-433}$.) Finally, some crystal trajectories are probably more common than others, in which case pd could decrease; for example, some crystals may stay close together as they fall and thus experience similar conditions.

The above result is consistent with our experience, but unfortunately is effectively impossible to disprove. For example, even in the first case above where $N_{cl} \sim 10^9$, the number of crystal comparisons is $\sim N_{cl}^2/2$, which, if each took 1 s, would take a total of $\sim 2 \times 10^{10}$ yr. So we may observe all crystals as unique even though the remaining ones

ACPD
8, 4407–4437, 2008

likely include some apparent copies[6].

7 Conclusions

To better understand snow crystal variety, we considered how snow crystals are viewed and how the crystals grow in a cloud. Specifically, we quantified the perceived crystal features using the crystal perimeter and resolvable growth intervals, and then estimated the shape diversity by analyzing the growth of a falling crystal. The resulting diversity was large, but not large enough to ensure that all crystals will appear unique at a typically viewed resolution. The main cause of the diversity was temperature deviations, arising from air-temperature inhomogeneities and deviations of updraft speed.

Snow crystals can be very diverse because their growth rate is sensitive to temperature. Those that start near –15°C are largest because the growth rate is a maximum and the fallspeed is a minimum near this temperature. Their large size gives them relatively large diversity, but the diversity peaks at slightly colder and slightly warmer temperatures (–15.4 and –14.4°C) due to maxima in temperature sensitivity near these temperatures. Thus, despite the need for greater knowledge of snow-crystal growth, we could identify some of the important properties that contribute to their seemingly endless variety.

[6] Although this had not been rigorously examined, some authors considered it obvious. For example, in 1901, W. A. Bentley wrote "Of the tens of thousands now filling the air, an infinitesimal proportion fall on this board; nor is there any good reason to doubt that when they started from equal heights on their journey earthward, many of the snow crystals were exactly alike in shape and size, and probably in density." (Harper's Monthly Magazine, December, 111 ,1901).

ACPD
8, 4407–4437, 2008

Appendix A Calculation of reference trajectories

$z(t)$ was calculated by summing $dz=(\bar{u}-v)dt$ for timesteps dt ranging from 4 to 0.1 s. At z=0, T=0°C so $T=T'z$ at each step. If z reached cloudtop (where T=–23°C), then dz=0 until $v>\bar{u}$. Only the T dependence of r was considered because r varies little with d and air pressure. The calculation ended when the crystal reached cloudbase at $T=T_f$. The resulting values of L_f, d_f, and n fluctuated with decreasing amplitude as dt decreased, so the final values were weighted averages from the various dt values with greater weight given to smaller dt results.

v values are unknown for crystals growing with varying temperature, so I used fits to measured, constant-T values of $v(T,t)$ as follows. I assumed that v primarily depended on d and crystal habit, the latter of which was fixed by the crystal's T_0 value. Thus, t in $v(T,t)$ was replaced by the time it would have taken the crystal to reach diameter d if it had remained at T_0; that is, $(d-d_0)/r(T_0)$. Also, the temperature was set to T_0. Thus, $v(T,t)\rightarrow v(T_0, (d-d_0)/r(T_0))$.

Appendix B Equations for r, v

Takahashi et al.'s (1991) data on r and v from were fit to the following functions. In units of μm/s,

$$r(T) = a_1 + (a_2 - a_3(T-T_m) + a_4(T-T_m)^2 - a_5(T-T_m)^3 + a_6(T-T_m)^4)^{-1},$$

where T_m=–14.8°C and values of a_i are in Table 3. In units of m/s,

$$v(T,t) = V_1(T,t)V_2(T),$$

where t is time in min and

$$V_1(T,t) = b_1 + b_2 \quad V_3(T)t^{(b3+t(V4(T)-b3)/(t+20)))},$$

$$V_2(T) = 1 + 0.3e^{-0.6(T+22)} - 0.21e^{-0.25(T+18)\wedge 2},$$

ACPD
8, 4407–4437, 2008

$V_3(T) = b_4 - b_5 \quad T + b_6 cos[c_1(T + 19) - c_2(T + 19)^2)]$,

$V_4(T) = c_3 + c_4 \quad T + 0.06 cos[c_5(T + c_6)]$,

and b_i and c_i are in Table 3. The sole consideration for the above functional forms was to obtain as good a fit to the data as possible.

Appendix C Determination of the distribution functions

Temperature values T_{ai-i}, with i labelling the data point, represented measurements at equally spaced points 8-mm apart in a 9.60-km-long dataset and 15-cm apart in a 4.05-km dataset. Figure 7a is a data sample. In a given data interval, DT_{ai-i} values were obtained by subtracting the average value from T_{ai-i}. To obtain the growth-perturbation curve Σ_{ai}, the DT_{ai-i} values were linearly interpolated and integrated. For u, the same method was used to obtain $D\bar{u}_i$ and then integrated to obtain Dz_i. Using $DT_{Du-i} = T' Dz_i$ (e.g., Fig. 7b), the DT_{Du} data were integrated to obtain Σ_{Du}.

To extract all relevant peaks from the jagged curves of Σ_{ai} (e.g., Fig. 7c,d), I did the following. If the largest peak (positive or negative) occurred at point x_1 with value p_1, then the original T_{ai-i} data were re-averaged over the two segments of i from 1 to x_1 and x_1 to the last value X. The new DT_{ai-i} values were used to make a new Σ'_{ai}. As the point x_1 is now an endpoint of both sets, Σ'_{ai} equals 0 at x_1 (e.g., Fig. 7d). But Σ'_{ai} will contain a new peak. Calling this peak point x_2 with peak value p_2, I again divided the set at this point. Assume that $x_2 > x_1$. The original set T_{ai-i} was then averaged over three segments: 1 to x_1, x_1 to x_2, and x_2 to X. This process continued, resulting in peak values p_1, p_2, p_3,..., with the values of p steadily decreasing. The iteration stopped when p was so low that no subsequent peak value could produce a feature ($p \sim 0.01$°C m). The p values were then used to make the peak distribution. By comparing peak distributions for segments of various lengths X, I found that the peak distribution for a given point p' was proportional to X. Thus, the function was scaled by the distance to give the peak distribution per meter F_{ai}. The same method was used for F_{Du}.

ACPD
8, 4407–4437, 2008

Acknowledgements. S. Malinowski and H. Siebert kindly supplied the temperature and updraft data; T. Takahashi let me use his crystal images; and M. Baker, D. Lamb, and D. Blanchard made manuscript suggestions.

References

Bentley, W. A.: Twenty years' study of snow crystals, Mon. Weather Rev. 21, 212–214, 1901.

Feller, W.: An Introduction to Probability Theory and its Applications, Vol. I, 3rd Edition, John Wiley & Sons, NY, 1968 (see end of §II.3.).

Frank, F. C.: Snow crystals, Contemp. Phys., 23, 3–22, 1982.

Hallett, J.: How snow crystals grow, Am. Sci., 72, 582–589, 1984.

Hallett, J. and Knight, C. A.: On the symmetry of snow dendrites, Atmos. Res., 32, 1–11, 1994.

Knight, C. and Knight, N.: Snow crystals, Sci. Am., 228 (1), 100–107, 1973.

Korolev, A. and Isaac, G. A.: Relative Humidity in Liquid, Mixed-Phase, and Ice Clouds, J. Atmos. Sci., 63, 2865–2880, 2006.

Nakaya, U.: Snow Crystals Natural and Artificial, Harvard University Press, Cambridge, 1954.

Nelson, J.: Branch growth and sidebranching in snow crystals, Cryst. Growth Des., 5, 1509–1525, 2005.

Shaw, R. A.: Supersaturation intermittency in turbulent clouds, J. Atmos. Sci., 57, 3452–3456, 2000.

Siebert, H., Wendisch, M., Conrath, T., Teichmann, U., Heintzenberg, J.: A New Tethered Balloon-Borne Payload for Fine-Scale Observations in the Cloudy Boundary Layer, Bound.-Lay. Meteorol., 106, 461–482, 2003.

Takahashi, T., Endoh, T., Wakahama, G., Fukuta, N.: Vapor diffusional growth of free-falling snow crystals between –3 and –23°C, J. Meteorol. Soc. Jpn., 69, 15–30, 1991.

Wolde, M. and Vali, G.: Polarimetric Signatures from Ice Crystals Observed at 95 GHz in Winter Clouds, Part II: Frequencies of Occurrence, J. Atmos. Sci., 58, 842–849, 2001.

Wood, S., Baker, M., and Calhoun, D.: New Model for the Vapor Growth of Hexagonal Ice Crystals in the Atmosphere, J. Geophys. Res., 106, 4845–4870, 2001.

Yamashita, A.: On the trigonal growth of ice crystals, J. Meteorol. Soc. Jpn., 51, 307–317, 1973.

Table 1. Trajectory results for d_f, L_f, S_0, and S_{ref}.

T_0 [°C]	–11	–13	–15	–17	–19
$d_f^{\dagger}$ [μm]	441	1843	7600	3919	2069
$L_f^{\dagger}$ [m]	686	1227	1850	1866	2009
$\delta d_0^{\dagger}$ [10^{-7} m]	96	52	38	2.9	3.2
$\delta T_0^{\dagger}$ [10^{-3}°C]	9.1	1.4	1.5	1.2	4.4
$\delta \bar{u}^{\dagger}$ [10^{-5} m/s]	110	27	5	25	100
$\delta T_f^{\dagger}$ [10^{-2}°C]	4.3	2.8	2.2	5.1	10
$S_0^{\ddagger}$	0.7	1.0	1.2	1.5	1.5
$S_{ref}^{\ddagger}$	7.5	9.3	10.1	9.1	7.5

† Baseline case (1 below), *res*=1 μm. (cloud is 2143-m thick).

‡ Average of cases 1–4:
{d_0 [μm], $\bar{u}$ [m/s], T_f [°C]}=1: {8, 0.12, –8}; 2: {1, 0.12, –8};3: {1,0.01, T_0+1}; 4: {40, 0.25, T_0+ 11}.

ACPD
8, 4407–4437, 2008

Table 2. Combinatorial parameters n and m.

T_0[°C]	–11	–13	–15	–17	–19
$n^{\dagger}$	48.8	229.9	467.5	213.0	88.6
$m^{\ddagger}$	220.6	921.3	3799.9	1959.7	1034.3
$\mathrm{Log}_{10}[2me/n]$	1.4	1.3	1.6	1.7	1.8

† Based on L_f from Table 1, and the average $F_{ai}+F_{Du}$ for the coldest and warmest parts of the trajectory.

‡ m=d_f/2res, with d_f from Table 1.

ACPD
8, 4407–4437, 2008

Table 3. Coefficients for fits to r and v.

i value	a_i	b_i	c_i
1	4.84×10^{-2}	2.04×10^{-3}	0.835
2	0.845	8.00×10^{-3}	2.06×10^{-2}
3	9.88×10^{-2}	0.973	0.866
4	0.613	2.96	1.48×10^{-2}
5	4.56×10^{-2}	2.24×10^{-2}	0.683
6	2.70×10^{-2}	0.788	10.2

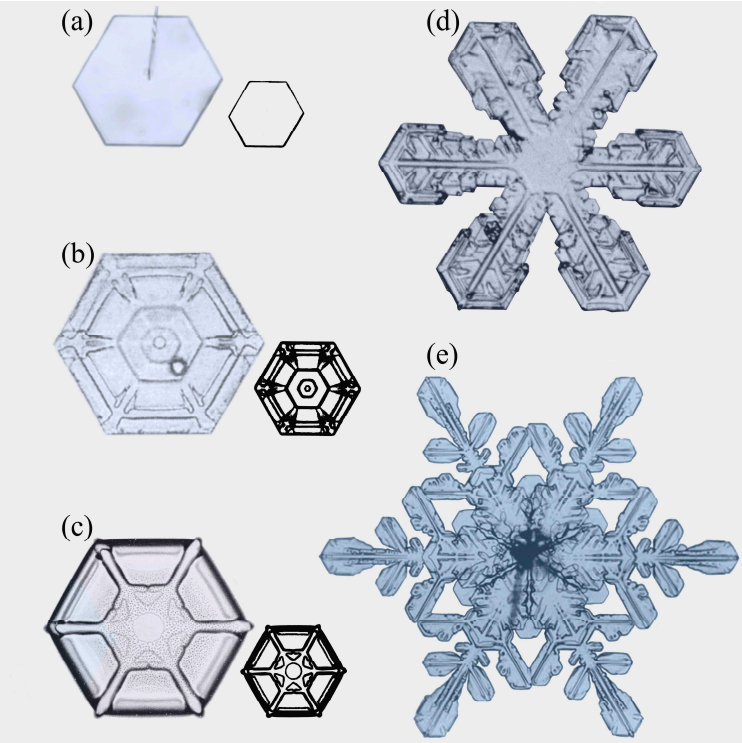

Fig. 1. Tabular snow crystals. **(a)** grew at low humidity near –9°C in constant conditions, suspended by a capillary (radial line). The perimeter shows the six prism faces. **(b)** grew in free-fall under nearly constant conditions of –12.2°C and liquid-water saturation (Takahashi et al., 1991). (c)–(e) are from natural snowfall. **(c)** likely grew in conditions like that for (b). Distinguishing features of (a)–(c) are sketched at right. **(d)** likely grew near –13°C, and **(e)** near –14°C. Photos (b)–(e) courtesy of T. Takahashi.

ACPD
8, 4407–4437, 2008

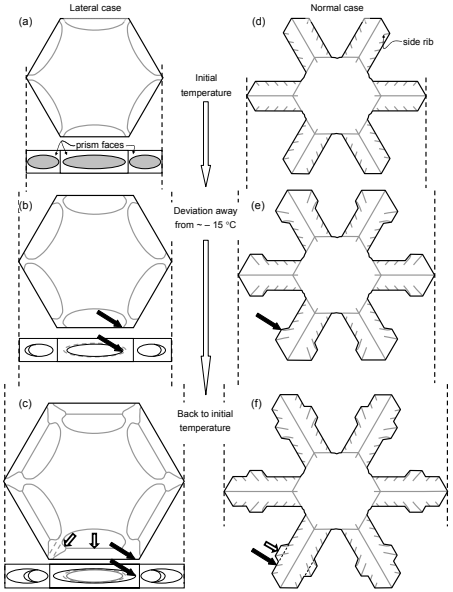

Fig. 2. Crystal features formed by growth changes in a cloud at liquid-water saturation. (a)–(c) Hollowed tabular crystal with growth changes *lateral* to the prism surface. **(a)** is the initial crystal. Front view beneath shows the pits in the three prism faces. In **(b)**, growth slows, as T moves away from the growth-rate peak near –15°C, narrowing the lip of the pit (filled arrow). In **(c)**, growth resumes at the faster rate as T returns to its previous value, thus widening the lip of the pit (filled arrow). Grey lines are features due to the growth change, here boundaries of the pits and ribs (vertical hollow arrow). (d)–(f) Stellar crystal with growth changes *normal* to the prism surface. **(d)** is the form from growth under constant conditions. Side ribs and longer main ribs are ridges on the branch underside (Nelson, 2005). Growth slows in **(e)**, as T moves away from the growth-rate peak, widening the tip (solid arrow), before resuming at the faster rate, at the previous T, and narrowing in **(f)** (solid arrow). Hollow arrows mark the features in both cases. If growth had not slowed, the features would instead follow the dashed lines.

ACPD
8, 4407–4437, 2008

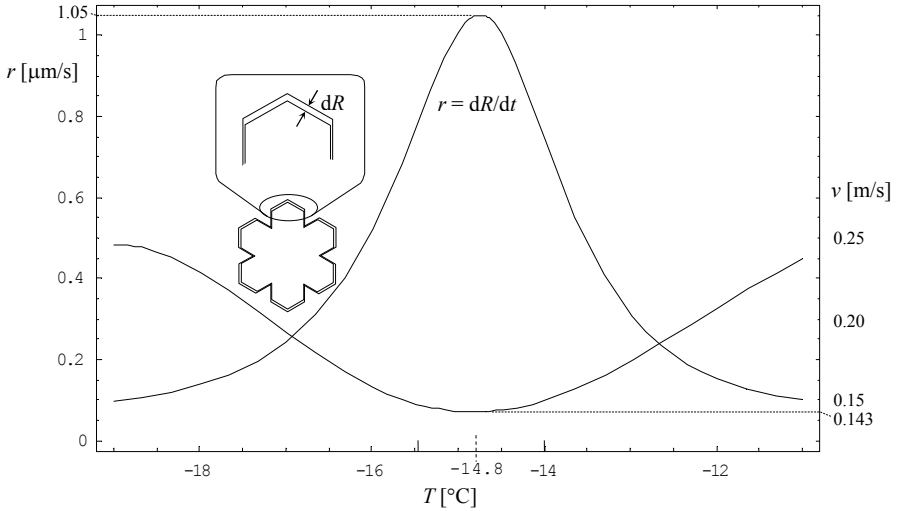

Fig. 3. Prism-face growth rates (left axis) and fallspeeds (right axis) for crystals at constant temperature. Curves are fits to Takahashi et al.'s (1991) data for crystals grown for 10 min. At later times, v increases, most rapidly at temperatures away from the peak, and r decreases slightly, mainly at temperatures away from the peak. (Functional forms are in Appendix B.) Marks on the abscissa mark peaks in r' and r. The basal-face growth rate (not shown) has a minimum where the prism-face has a maximum.

ACPD
8, 4407–4437, 2008

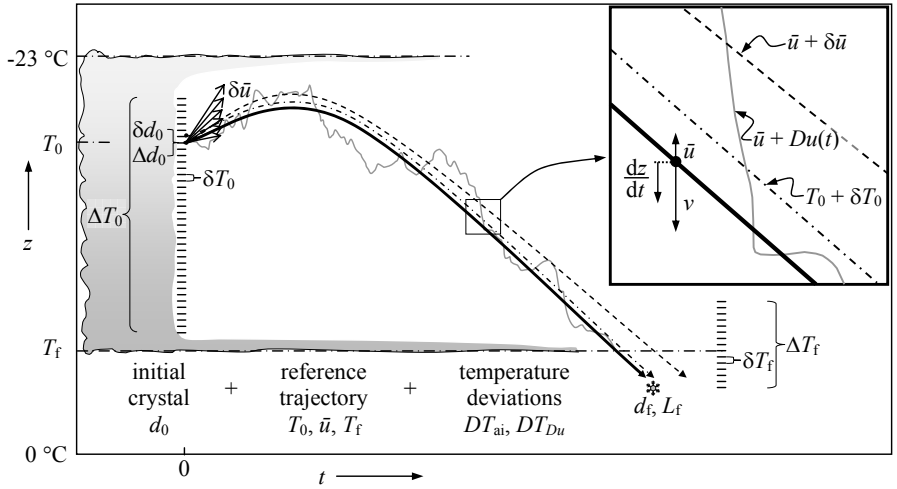

Fig. 4. Model of reference trajectories. In a trajectory $z(t)$, a crystal nucleates with diameter d_0 at T_0 in an updraft $\bar{u}$ then falls at speed $\bar{u}-v$ until reaching cloudbase at temperature T_f (solid curve). Each resolvable variation δd_0, δT_0, $\delta\bar{u}$, and δT_f results in a final diameter d_f that changes by $\pm 2res$ (dashed curves). Variable ranges are Δd_0, ΔT_0, $\Delta\bar{u}$, and ΔT_f, making the number of distinct d_0-reference classes $N_0 N_{\text{ref}} = (\Delta d_0/\delta d_0)(\Delta T_0/\delta T_0 \Delta\bar{u}/\delta\bar{u}\Delta T_f/\delta T_f)$. Values are in Table 1. DT_{ai} and DT_{Du} (from updraft deviations Du – dotted curve) are temperature deviations that further alter crystal shape. For each trajectory, the number N_{dev} of deviation-caused shape changes depends on d_f/res, the final pathlength L_f, and the number of relevant deviations/meter $(F_{ai}+F_{Du})$.

ACPD
8, 4407–4437, 2008

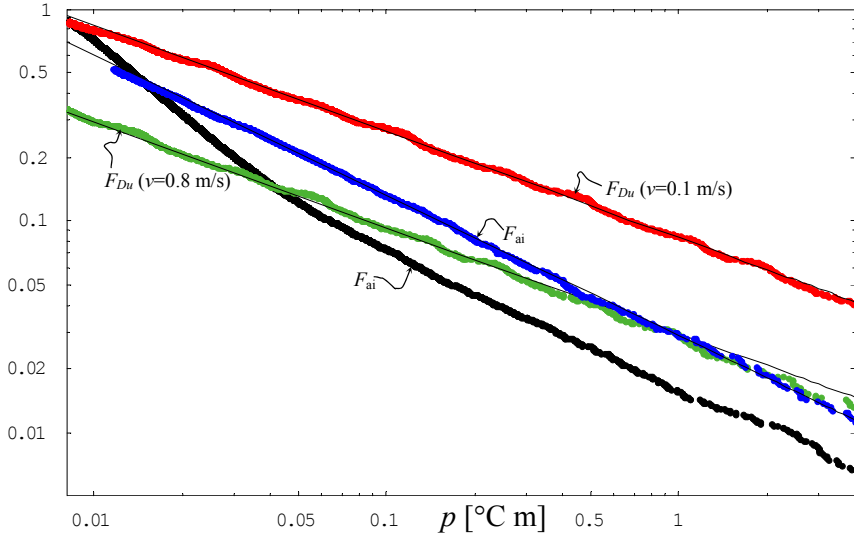

Fig. 5. Temperature deviation distribution functions F_{ai} and F_{Du}. All functions are from measurements at 15-cm intervals except the lower F_{ai} one, which instead had 8-mm intervals. Also shown are fits F_{ai}=0.0287 $p^{-0.66}$ and F_{Du}=0.0262 $p^{-0.50}v^{-0.5}$.

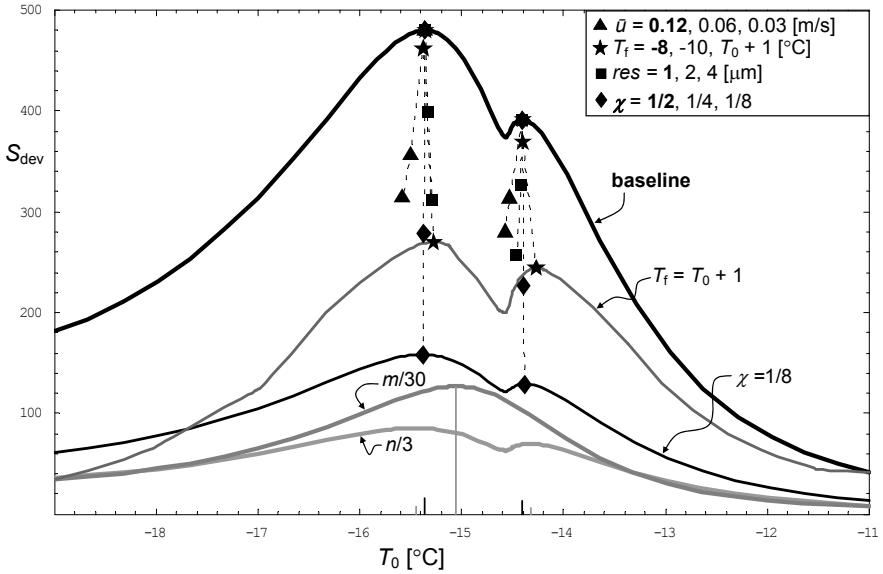

Fig. 6. Shape diversity S_{dev}. The upper black curve, the baseline case (bold values in legend), is derived from the grey curves of m (reduced 30-fold) and n (reduced 3-fold). Solid triangles, stars, squares, and diamonds mark peak positions for other $\bar{u}$, T_f, χ, or *res* values. Full curves show cases χ=1/8 and T_f=T_0+1. Vertical lines on the abscissa are peak positions and relative magnitudes for the baseline case (black lines), the value of m (long grey line), and the value of n (short grey lines).

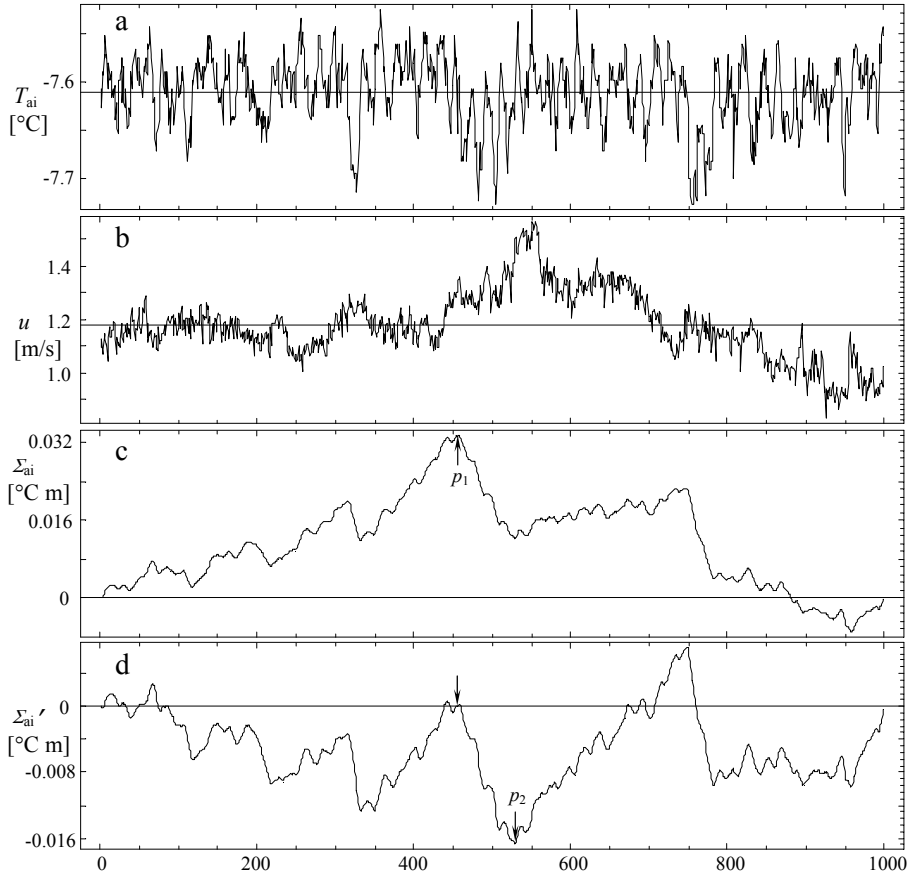

Fig. 7. Analysis of deviations. **(a)** Segment of T_{ai} data. **(b)** Segment of $\bar{u}+Du$ data. **(c)** Integrated temperature Σ_{ai} from (a). Maximum peak p_1 is marked. **(d)** Σ_{ai} after the peak in (c) was removed by breaking the segment into pre-peak and post-peak segments as described in Appendix C. New maximum peak p_2 is marked.

ACPD
8, 4407–4437, 2008